Switching Dynamics of Ferroelectric Zr-Doped HfO$_2$

Cristobal Alessandri, *Student Member, IEEE*, Pratyush Pandey, Angel Abusleme, *Member, IEEE*,
and Alan Seabaugh, *Fellow, IEEE*

Abstract—**Ferroelectric Zr-doped HfO$_2$ (HZO) is a promising candidate for steep slope transistors and memory technology. For these applications, it is essential to understand and optimize the switching dynamics of the ferroelectric film. In this letter, we characterize the polarization reversal of an 8 nm-thick HZO film deposited by the atomic layer deposition with voltage pulses varying in amplitude (0.8–2 V) and duration (200 ns–7.6 ms). We show that the measurements are well described by a nucleation limited switching model, which enables extraction of the minimum switching time and the probability distribution of local electric field variations in the polycrystalline film. The close model fit spanning 5 orders of magnitude in pulse duration indicates the applicability of this model to HZO. This characterization framework can be used to quantify, compare, and optimize the switching dynamics of ferroelectric HZO.**

Index Terms—**Ferroelectric devices, analytical models, hafnium compounds.**

I. INTRODUCTION

THE discovery of ferroelectricity in the CMOS-compatible HfO$_2$ material system [1] has led to a variety of applications including memory [2]–[4], steep slope transistors [5], [6], and neuromorphic computing [7], [8]. Several studies have analyzed the effect of growth and annealing conditions on the FE properties of Zr-doped HfO$_2$ (HZO), such as the Zr concentration [9], [10], electrode material [11], [12] and annealing temperature [13], [14]. These studies usually focus on properties that can be directly measured from the polarization-voltage (P-V) loops, such as the remanent polarization and endurance, but provide limited insight into the FE dynamics or speed limitations, a subject that is widely
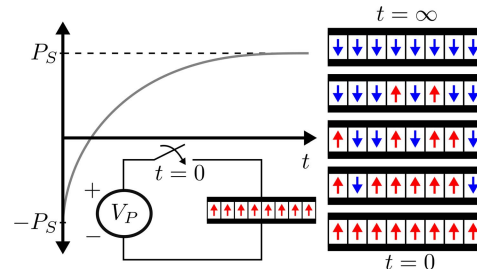
Fig. 1. Polarization reversal of a polycrystalline FE film. Starting from a fully polarized state $-P_S$, a positive voltage is applied at $t = 0$. The FE grains switch and increasingly align until the FE reaches the fully polarized state $+P_S$.

debated [15], [16]. On the other hand, nucleation limited switching (NLS) models for polarization reversal provide an accurate description of the switching transient of FE thin films, and have been experimentally validated in other material systems [17]–[19]. Although it has been shown that the polarization reversal of ferroelectric HfO$_2$ occurs in the nucleation limited regime [20]–[22], only one prior study reports parameter extraction by applying an NLS model to Al-doped HfO$_2$ [23].

In this work, we show that the NLS model [17] provides a good description of the polarization reversal of HZO films, under the assumption of a distribution of switching times that originate from variations in the local electric field [19]. We extract the probability distribution that characterizes the electric field variations and the parameters that govern the polarization dynamics. This characterization framework can be used to guide the optimization of the HZO material system.

II. MODEL FOR POLARIZATION REVERSAL IN THIN-FILM FERROELECTRICS

Figure 1 depicts the polarization reversal of a polycrystalline FE thin film, which is composed of many grains with fixed grain walls. When all the grains are polarized in the same direction, a saturation polarization P_S is obtained (C/m^2). Starting from the $-P_S$ state, if a positive voltage is applied at $t = 0$, the FE grains will start to switch polarization until the whole FE reaches the $+P_S$ state. A stable partially polarized state is obtained by pulsing the applied voltage for a time t short enough so only a fraction of the FE grains are able to switch. The NLS model was proposed to account for multigrain polarization by characterizing the thin film as an ensemble of elementary regions that switch independently with a distribution of switching times [17]. This distribution of switching times was later attributed to
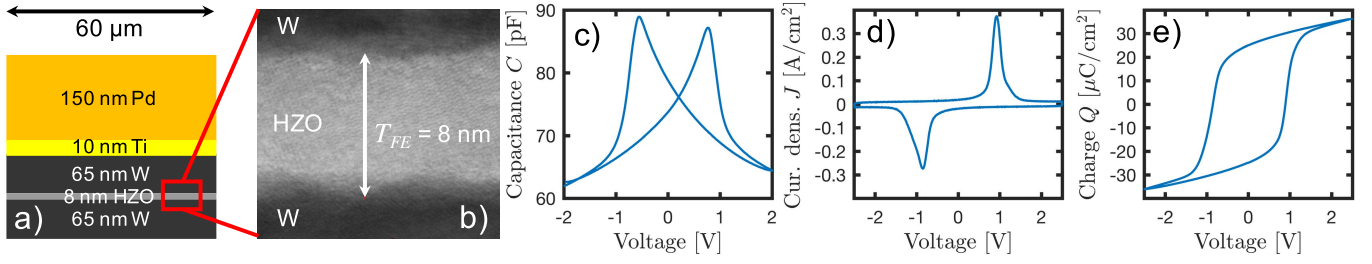
Fig. 2. a) Cross section and b) TEM of 8 nm thick $Hf_{0.5}Zr_{0.5}O_2$ FE capacitor with 60 μm-diameter top electrode. c) Capacitance-Voltage measurements with 1 V/s sweep rate and 30 mV, 100 kHz AC signal. d) Current-voltage characteristic of $Hf_{0.5}Zr_{0.5}O_2$, measured with a 2.5 V triangular waveform with 4 ms period. e) P-V loop obtained by integrating the current-voltage characteristic.

variations in the local electric field when a uniform external field is applied, due to impurities or crystal defects [18], or the intrinsic inhomogeneity of the FE film [19]. The field-dependent NLS model can be summarized as follows: The switching of a single elementary region is described by a stretched exponential with parameter β [18], [19]

$$p(t, \tau) = 1 - \exp\left\{-\left(\frac{t}{\tau}\right)^{\beta}\right\}. \quad (1)$$

The characteristic switching time τ is a function of the local field E and an activation field E_a, expressed by the empirical relation [19], [24]

$$\tau(E_a, E) = \tau_{\infty}\exp\left\{\left(\frac{E_a}{E}\right)^{\alpha}\right\}, \quad (2)$$

where τ_{∞} is the time constant obtained for an infinite applied field, and α is an empirical parameter. Assuming an inhomogeneous and field-independent dielectric permittivity, the local electric field value is expressed as $E = \eta E_{ext}$, where E_{ext} is the constant applied field and η is a random variable with probability density function (PDF) $f(\eta)$ and unity mean, defined in the $[0, \infty)$ interval [19]. As a result, the polarization reversal from $-P_S$ to $+P_S$ is computed as

$$P(E_{ext}, t) = -P_S + 2P_S\int_{0}^{\infty} p(t, \tau(E_a, \eta E_{ext}))f(\eta)d\eta \quad (3)$$

With this mathematical formulation, the FE film is characterized by the parameters P_S, E_a, β, α, τ_{∞} and the probability density function $f(\eta)$.

III. EXPERIMENTAL RESULTS AND PARAMETER EXTRACTION

The cross section and transmission electron microscopy (TEM) of an 8 nm FE W/HZO/W capacitor are shown in Fig. 2a) and b). The device fabrication started by sputtering 65 nm W on a Si wafer. The HZO was deposited by atomic layer deposition at 300 °C with tetrakis(ethylmethyl-amino)hafnium and tetrakis(ethylmethylamino)zirconium precursors, and water vapor as the oxidant. The HZO was then capped with 65 nm of sputtered W and annealed at 500 °C for 30 s in N₂. Then, 60 μm-diameter dots were deposited by shadow mask evaporation of Ti/Pd. Finally, the top W and HZO were etched using the Ti/Pd electrodes as a hard mask. A Hf:Zr ratio of 1:1 was verified with energy dispersive X-ray linescans.

Electrical measurements were performed with a Keithley 4200 parameter analyzer with a 4225-PMU pulse measurement
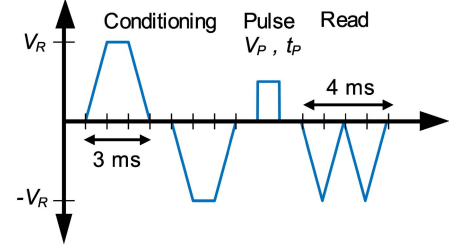

Fig. 3. Measurement protocol for polarization reversal. Conditioning pulses of amplitude $V_R = 2.5$ V are applied to reset the FE. A programming pulse of varying width and amplitude is applied, and the polarization is measured by two pulses of amplitude $V_R = 2.5$ V.

unit and two 4225-RPM remote preamplifiers. The experimental setup and the capacitor diameter were designed so that the partial polarization measurements are not limited by RC delays. The combined resistance of the 50 Ω output resistance of the remote amplifier and the series resistance of the probes was measured to be 54 Ω, which with the measured capacitance (Fig. 2c)) results in a time constant in the order of 5 ns. A 2.5 V triangular waveform with 4 ms period was applied for 500 cycles for wake up. The current-voltage and P-V characteristics are shown in Fig. 2d) and e), measured after wake up. The measurement sequence performed to characterize the polarization reversal is depicted in Fig. 3. Conditioning pulses of amplitude $V_R = 2.5$ V are applied to reset the FE. The programming pulse width (t_P) was stepped from 200 ns to 7.6 ms in increments of 1.5×, then the amplitude (V_P) was stepped from 0.8 V to 2 V in increments of 100 mV. The polarization is measured by two consecutive negative pulses of amplitude $V_R = 2.5$ V and 1 ms rise time. The first pulse polarizes the capacitor back to the $-P_S$ state, and produces a current due to the linear capacitance and the polarization current of the switched domains. The displacement current due to the linear capacitance alone is measured by the second pulse, where there is no polarization current. The current difference is integrated to calculate the partial polarization. The pulse amplitude V_P is translated to field E_{ext} by dividing by the film thickness (T_{FE}). Figure 4 shows the polarization reversal measurements (dots) and the fitted model (solid lines) as a function of pulse width and pulse amplitude. In addition, polarization measurements with 2.5 V pulses (diamonds) are shown to verify that the conditioning and read pulses produce a saturated polarization.

The distribution of local field variations $f(\eta)$ was extracted from measurements with the method presented in [19]. The logarithmic derivative of the polarization with respect to the
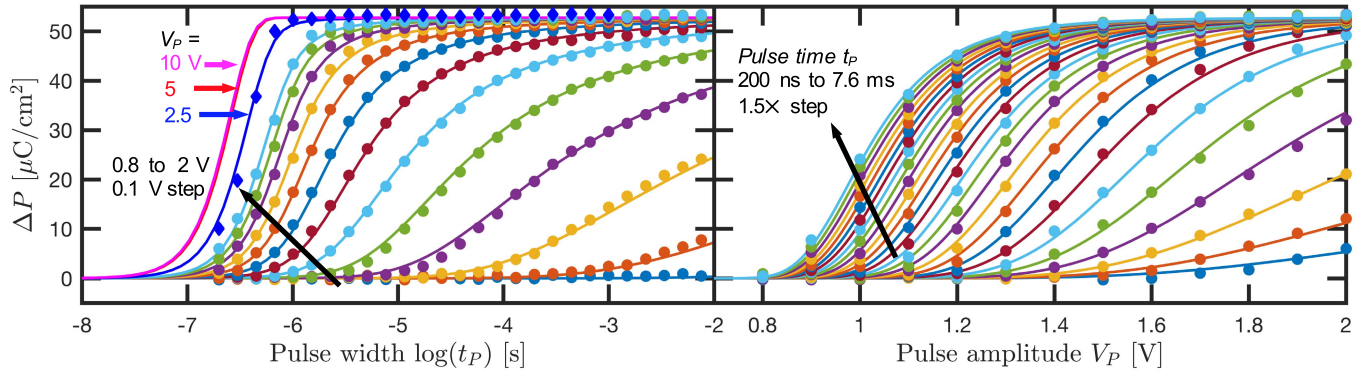
Fig. 4. Measured partial polarization (dots) vs. pulse width (left) and pulse amplitude (right) show close agreement with model (solid line) over 5 decades of pulse times. Extracted parameters are $P_S = 26.4$ μC/cm^2, $\tau_\infty = 236$ ns, $E_a = 2.42$ MV/cm, $\alpha = 3.73$ and $\beta = 2.06$. Measurements with 2.5 V pulse amplitude (diamonds) were not used for parameter extraction, which demonstrates the predictive capability of the model.
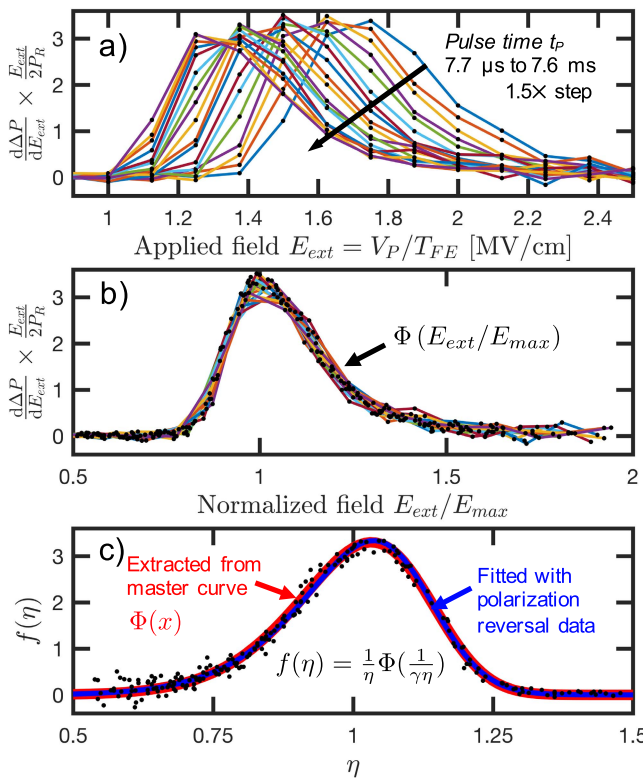

Fig. 5. Extraction of the distribution of local field variations $f(\eta)$ [19]. a) Derivatives of the polarization with respect to applied field. b) The derivatives overlap into a master curve $\Phi(x)$ when the x-axis is normalized by the field at which the derivatives are peaked. c) Distribution of local fields obtained from $\Phi(x)$ (red), with the proportionality constant γ derived from condition of unity mean. The same distribution was obtained by fitting the distribution parameters directly from the polarization reversal data (blue).

applied field exhibits a maximum at a certain field E_{max} that depends on the pulse time t_P, as shown in Fig. 5a). When the x-axis is normalized by E_{max} for each pulse time t_P, the derivatives overlap into a master curve $\Phi(x)$ (Fig. 5b)). The distribution $f(\eta)$ is obtained from the master curve as

$$f(\eta) = \frac{1}{\eta}\Phi\left(\frac{1}{\gamma\,\eta}\right), \qquad (4)$$

where γ is a proportionality constant derived from the condition of unity mean [19]. As shown in Fig. 5c), the data is well described by a generalized beta distribution of type 2,

whose PDF is

$$GB2(\eta|a,b,p,q) = \frac{\frac{|a|}{b}\left(\frac{\eta}{b}\right)^{ap-1}}{B(p,q)\left(1+\left(\frac{\eta}{b}\right)^a\right)^{p+q}}, \qquad (5)$$

where $B(p,q)$ is the beta function. The distribution parameters are $a = 9.0986$, $b = 1.3935$, $p = 1.1101$ and $q = 15.197$. The parameters P_S, E_a, β, α and τ_∞ were then extracted by performing a least square fit of Eq. (3) with the polarization reversal data. Alternatively, once the analytic form of the distribution is known, its parameters can be extracted with the least square fit directly from the polarization reversal data. The resulting distribution is not sensitive to the extraction method, as shown in Fig. 5c), and the fitted parameters vary by less than 1%, which underscores the physicality of the model. Furthermore, the fitted model is able to predict the measured polarization reversal with 2.5 V pulses, which was not used for parameter extraction.

According to Eq. (2), as the applied field increases, τ asymptotically reaches its minimum value $\tau_\infty = 236$ ns, which imposes a hard limit on the switching speed. This limitation is shown in Fig. 4 by extrapolating the pulse amplitude to 2.5, 5 and 10 V. The relative speed at which the FE grains switch is determined by the spread of the distribution of local field variations: grains at the higher end of the distribution have a smaller time constant and will switch sooner than those with η closer to zero. Therefore, a large variance in the local field distribution favors partial polarization, but is not desirable for fast transitions between saturated states ($\pm P_S$). Furthermore, a narrow distribution is needed for memory writing schemes that leverage the nonlinearity of the FE response to applied field [4].

IV. CONCLUSION

We modeled and characterized the polarization reversal of HZO. We show that the field-dependent NLS model provides a comprehensive description of the polarization reversal of HZO films for varying pulse amplitudes and pulse width spanning over 5 decades. We extracted the probability distribution that characterizes the local electric field variations in the FE film, and the parameters that govern the polarization dynamics. This characterization framework provides the tools to quantify, compare and optimize the switching dynamics and the nonlinear response to applied field of HZO films.

REFERENCES

[1] T. S. Böscke, J. Müller, D. Bräuhaus, U. Schröder, and U. Böttger, "Ferroelectricity in hafnium oxide: CMOS compatible ferroelectric field effect transistors," in *IEDM Tech. Dig.*, Dec. 2011, pp. 24.5.1–24.5.4., doi: 10.1109/IEDM.2011.6131606.

[2] X. Li, S. George, K. Ma, W. Y. Tsai, A. Aziz, J. Sampson, S. K. Gupta, M. F. Chang, S. Liu, S. Datta, and V. Narayanan, "Advancing nonvolatile computing with nonvolatile NCFET latches and flip-flops," *IEEE Trans. Circuits Syst. I, Reg. Papers*, vol. 64, no. 11, pp. 2907–2919, Nov. 2017, doi: 10.1109/TCSI.2017.2702741.

[3] Y. Li, R. Liang, J. Wang, Y. Zhang, H. Tian, H. Liu, S. Li, W. Mao, Y. Pang, Y. Li, Y. Yang, and T. Ren, "A ferroelectric thin film transistor based on annealing-free HfZrO film," *IEEE J. Electron Devices Soc.*, vol. 5, no. 5, pp. 378–383, Sep. 2017, doi: 10.1109/JEDS.2017.2732166.

[4] A. Sharma and K. Roy, "1T non-volatile memory design using sub-10 nm ferroelectric FETs," *IEEE Electron Device Lett.*, vol. 39, no. 3, pp. 359–362, Mar. 2018, doi: 10.1109/LED.2018.2797887.

[5] D. Kwon, K. Chatterjee, A. J. Tan, A. K. Yadav, H. Zhou, A. B. Sachid, R. dos Reis, C. Hu, and S. Salahuddin, "Improved subthreshold swing and short channel effect in FDSOI n-channel negative capacitance field effect transistors," *IEEE Electron Device Lett.*, vol. 39, no. 2, pp. 300–303, Feb. 2017, doi: 10.1109/LED.2017.2787063.

[6] A. Aziz, E. T. Breyer, A. Chen, X. Chen, S. Datta, S. K. Gupta, M. Hoffmann, X. S. Hu, A. Ionescu, M. Jerry, T. Mikolajick, H. Mulaosmanovic, K. Ni, M. Niemier, I. O'Connor, A. Saha, S. Slesazeck, S. K. Thirumala, and X. Yin, "Computing with ferroelectric FETs: Devices, models, systems, and applications," in *Proc. Design, Automat. Test Eur. Conf. Exhib. (DATE)*, Mar. 2018, pp. 1289–1298, doi: 10.23919/DATE.2018.8342213.

[7] E. W. Kinder, C. Alessandri, P. Pandey, G. Karbasian, S. Salahuddin, and A. Seabaugh, "Partial switching of ferroelectrics for synaptic weight storage," in *Proc. Device Res. Conf. (DRC)*, Jun. 2017, pp. 1–2, doi: 10.1109/DRC.2017.7999427.

[8] S. Oh, T. Kim, M. Kwak, J. Song, J. Woo, S. Jeon, I. K. Yoo, and H. Hwang, "HfZrO$_X$-based ferroelectric synapse device with 32 levels of conductance states for neuromorphic applications," *IEEE Electron Device Lett.*, vol. 38, no. 6, pp. 732–735, Jun. 2017, doi: 10.1109/LED.2017.2698083.

[9] M. H. Park, H. J. Kim, Y. J. Kim, Y. H. Lee, T. Moon, K. D. Kim, S. D. Hyun, F. Fengler, U. Schroeder, and C. S. Hwang, "Effect of Zr content on the wake-up effect in Hf$_{1-x}$Zr$_x$O$_2$ Films," *ACS Appl. Mater. Interfaces*, vol. 8, no. 24, pp. 15466–15475, 2016, doi: 10.1021/acsami.6b03586.

[10] G. Karbasian, A. Tan, A. Yadav, E. M. H. Sorensen, C. R. Serrao, A. I. Khan, K. Chatterjee, S. Kim, C. Hu, and S. Salahuddin, "Ferroelectricity in HfO$_2$ thin films as a function of Zr doping," in *Proc. Int. Symp. VLSI Technol., Syst. Appl. (VLSI-TSA)*, Apr. 2017, pp. 1–2, doi: 10.1109/VLSI-TSA.2017.7942488.

[11] G. Karbasian, R. dos Reis, A. K. Yadav, A. J. Tan, C. Hu, and S. Salahuddin, "Stabilization of ferroelectric phase in tungsten capped Hf$_{0.8}$Zr$_{0.2}$O$_2$," *Appl. Phys. Lett.*, vol. 111, no. 2, pp. 022907-1–022907-4, Jun. 2017, doi: 10.1063/1.4993739.

[12] Y.-C. Lin, F. McGuire, and A. D. Franklin, "Realizing ferroelectric Hf$_{0.5}$Zr$_{0.5}$O$_2$ with elemental capping layers," *J. Vac. Sci. Technol. A, Vac. Surf. Films*, vol. 36, no. 1, p. 011204, 2018, doi: 10.1116/1.5002558.

[13] S. J. Kim, D. Narayan, J.-G. Lee, J. Mohan, J. S. Lee, J. Lee, H. S. Kim, Y.-C. Byun, A. T. Lucero, C. D. Young, S. R. Summerfelt, T. San, L. Colombo, and J. Kim, "Large ferroelectric polarization of TiN/Hf$_0$.5Zr$_0$.5O$_2$/TiN capacitors due to stress-induced crystallization at low thermal budget," *Appl. Phys. Lett.*, vol. 111, no. 24, p. 242901, 2017, doi: 10.1063/1.4995619.

[14] M. H. Park, H. J. Kim, Y. J. Kim, W. Lee, T. Moon, and C. S. Hwang, "Evolution of phases and ferroelectric properties of thin Hf$_{0.5}$Zr$_{0.5}$O$_2$ films according to the thickness and annealing temperature," *Appl. Phys. Lett.*, vol. 102, no. 24, p. 242905, 2013, doi: 10.1063/1.4811483.

[15] K. Chatterjee, A. J. Rosner, and S. Salahuddin, "Intrinsic speed limit of negative capacitance transistors," *IEEE Electron Device Lett.*, vol. 38, no. 9, pp. 1328–1330, Sep. 2017, doi: 10.1109/LED.2017.2731343.

[16] J. A. Kittl, B. Obradovic, D. Reddy, T. Rakshit, R. M. Hatcher, and M. S. Rodder, "On the validity and applicability of models of negative capacitance and implications for MOS applications," *Appl. Phys. Lett.*, vol. 113, no. 4, p. 042904, 2018, 10.1063/1.5036984.

[17] A. K. Tagantsev, I. Stolichnov, N. Setter, J. S. Cross, and M. Tsukada, "Non-Kolmogorov-Avrami switching kinetics in ferroelectric thin films," *Phys. Rev. B, Condens. Matter*, vol. 66, p. 214109, Dec. 2002, doi: 10.1103/PhysRevB.66.214109.

[18] J. Y. Jo, H. S. Han, J.-G. Yoon, T. K. Song, S.-H. Kim, and T. W. Noh, "Domain switching kinetics in disordered ferroelectric thin films," *Phys. Rev. Lett.*, vol. 99, no. 26, pp. 267602-1–267602-4, 2007, doi: 10.1103/PhysRevLett.99.267602.

[19] S. Zhukov, Y. A. Genenko, O. Hirsch, J. Glaum, T. Granzow, and H. von Seggern, "Dynamics of polarization reversal in virgin and fatigued ferroelectric ceramics by inhomogeneous field mechanism," *Phys. Rev. B, Condens. Matter*, vol. 82, no. 1, pp. 014109-1–014109-8, 2010, doi: 10.1103/PhysRevB.82.014109.

[20] S. Mueller, S. R. Summerfelt, J. Müller, U. Schroeder, and T. Mikolajick, "Ten-nanometer ferroelectric Si:HfO$_2$ films for next-generation FRAM capacitors," *IEEE Electron Device Lett.*, vol. 33, no. 9, pp. 1300–1302, Sep. 2012, doi: 10.1109/LED.2012.2204856.

[21] J. Müller, T. S. Böscke, S. Müller, E. Yurchuk, P. Polakowski, J. Paul, D. Martin, T. Schenk, K. Khullar, A. Kersch, W. Weinreich, S. Riedel, K. Seidel, A. Kumar, T. M. Arruda, S. V. Kalinin, T. Schlösser, R. Boschke, R. van Bentum, U. Schröder, and T. Mikolajick, "Ferroelectric hafnium oxide: A CMOS-compatible and highly scalable approach to future ferroelectric memories," in *IEDM Tech. Dig.*, Dec. 2013, pp. 10.8.1–10.8.4., doi: 10.1109/IEDM.2013.6724605.

[22] H. Mulaosmanovic, J. Ocker, S. Müller, U. Schroeder, J. Müller, P. Polakowski, S. Flachowsky, R. van Bentum, T. Mikolajick, and S. Slesazeck, "Switching kinetics in nanoscale hafnium oxide based ferroelectric field-effect transistors," *ACS Appl. Mater. Interfaces*, vol. 9, no. 4, pp. 3792–3798, 2017, doi: 10.1021/acsami.6b13866.

[23] N. Gong, X. Sun, H. Jiang, K. S. Chang-Liao, Q. Xia, and T. P. Ma, "Nucleation limited switching (NLS) model for HfO$_2$-based metal-ferroelectric-metal (MFM) capacitors: Switching kinetics and retention characteristics," *Appl. Phys. Lett.*, vol. 112, no. 26, p. 262903, 2018, doi: 10.1063/1.5010207.

[24] J. F. Scott, L. Kammerdiner, M. Parris, S. Traynor, V. Ottenbacher, A. Shawabkeh, and W. F. Oliver, "Switching kinetics of lead zirconate titanate submicron thin-film memories," *J. Appl. Phys.*, vol. 64, no. 2, pp. 787–792, 1988, doi: 10.1063/1.341925.